Journal of Materials and Engineering Structures

Research Paper

Ripening of the AlSi9Cu3ZnMg alloy - mechanical and microstructural characterisation

Ahmed HAKEM [a,*], ***Farid ASMA*** [b]

[a] *Laboratory of Mechanics, Structures and Energetics, Mouloud Mammeri University, Tizi-Ouzou, Algeria*

[b] *Laboratory of Elaboration, Characterisation of Materials and Modelisation , Mouloud Mammeri University, Tizi-Ouzou, Algeria*

ARTICLE INFO

Article history :

Received : 3 November 2021

Revised : 28 July 2022

Accepted : 10 August 2022

Keywords:

Aluminium alloys

Ripening

Hardening

Microstructure.

ABSTRACT

Recovered aluminium has poor mechanical properties, to improve them considerably, three main factors have been considered. The first is to add four very low-density elements to the recovered aluminium, including 9% silicon, 3% copper and some traces of zinc and magnesium less than 1% (≤ 1% Zinc, ≤ 1% Mg), which produces the non-standardized casting alloy $AlSi_9Cu_3ZnMg$. Then, in order to obtain a fine microstructure, a gravity die-casting is carried out in the as-cast state noted: F. Finally, to further increase the strength of the F-state and essentially obtain high elasticity stresses, high rigidity modulus with low deformations, the $AlSi_9Cu_3ZnMg$ alloy composed of 60% scrap and 40% new ingots, is subjected to structural hardening by varying the ripening time for 24 hours in increments of 2 hours, thus giving rise to precipitates of various kinds which impede the dislocations sliding.

The results thus obtained show that the cured state for 12 hours (M12h) is a good compromise between good strength and maximum ductility.

1 Introduction

The recovery and development of aluminium alloy wastes is of major importance from the technical and economic point of view as well as the protection of the environment. The sorting of these wastes mainly composed of 40% of new $AlSi_7Mg$ ingots and 60% of scrap, broken and worn parts (supply, evacuation, regulation appendages, defective parts), identified and manufactured by the National Company of Industrial Vehicles (SNVI an aluminium foundry unit), was carried out manually by the master founders.

The present study aims to determine the influence of the ripening time of the metal parts, components of the SNVI (Aluminium Foundry Unit) of Rouïba on the behaviour and the damage in traction, the Brinell hardness, microhardness,

* *Corresponding author. Tel.: +213 554970920.*
E-mail address: hakem_ahmed.hamid@ummto.dz

e-ISSN: 2170-127X,

RESEARCH REVIEW of Sciences and Technologies

impact strength [1-5] and microstructure [6-8] of the chemically designated $AlSi_9Cu_3ZnMg$ die-cast alloy [9-12] by gravitation in fifteen material states: as-cast noted: F, quenched noted: T and variation of the ripening time in steps of 2 hours respectively designated M0h to M24 hours.

The addition of 9% silicon, a percentage of copper (3% Cu), Zn and Mg (≤ 1% Zn, ≤ 1% Mg) to aluminium are the main agents for improving the mechanical characteristics [1-5, 13, 14] in addition to the specific heat treatments [15-22] that reveal precipitates [23, 24] of different kinds that hinder the movement of dislocations [25, 26].

Alloys of the Al-Si range [26-29] play a special role in the manufacture and production of many industrial parts. Being able to support large mechanical loads and having a good resistance to corrosion and oxidation by the addition of zinc, they are very much employed as accessories in several realizations (cylinder heads, frames, bodies, pulleys, casings.).

In addition to their high characteristics, these alloys have good casting properties, the increase in silicon content results in good castability and excellent mould filling ability, which is an important characteristic for casting large parts or for filling moulds with complex geometries [1, 27, 28].

In order to further increase the strength characteristics of the as-cast state noted: F to obtain essentially high yield strength, high rigidity modulus with low strains and the $AlSi_9Cu_3ZnMg$ alloy will be subjected to specific ripening treatments.

On the other hand, the mechanical characterization of this alloy is required because it is essentially used a fterwards for the calculations of the design engineer at the engineering office level for the sizing of the parts subjected to the various external stresses [1, 15, 16, 22].

Unalloyed aluminium having very low mechanical properties, leads to the addition of four very low density elements including 9% silicon, 3% copper and some traces of zinc and magnesium less than 0.1% (≤ 0.1% Zinc and Mg) to improve its properties and thus obtain a super light $AlSi_9Cu_3ZnMg$ alloy. These four addition elements (Si, Cu, Zn, Mg) can be in solid solution substitution by taking the place of aluminium atoms in the grid. Their size is smaller or larger than the aluminium atom, which disturbs the grid becoming more difficult, be deformed. The foundry alloy $AlSi_9Cu_3ZnMg$ under study is an alloy with a set of properties that in many circumstances make it an essential and irreplaceable material. These include the addition of a high percentage of silicon and copper and a low percentage of zinc and magnesium, which are largely the main vectors and agents for improving mechanical characteristics, combined with very good corrosion resistance.

To further increase these properties, the alloy will be both die-cast and subjected to specific heat treatments leading to a finer structure [2, 3, 6, 29].

2 Experimental procedures

2.1 Research material

2.1.1 Primary base material

In all our experiments, we used the recovered aluminium based alloy containing 9% silicon, 3% copper in mass percent, zinc and magnesium less than 1% (by mass) and a few traces of impurities, elaborated at the aluminium smelting unit and provided free of charge by SNVI [27-29].

After analysis, the specimens cast in metal shells by gravity have the following chemical composition:

Table 1 – Results of the chemical analysis after control on shell-cast specimens

Chemical elements	Si	Cu	Zn	Mg	Ni	Mn	Fe
% according to analysis	8,27	2,48	0,96	0,41	0,31	0,25	1,07

2.1.2 Elaboration of the foundry alloy $AlSi_9Cu_3ZnMg$ object of research

$AlSi_9Cu_3ZnMg$ gives safe, reproducible and standard-compliant results.

The composition below corresponds to the composition tolerances in die-castings.

Table 2 – Composition of $AlSi_7Mg$ ingots delivered by the French Aluminium

Chemical Elements	Fe	Si	Cu	Zn	Mg	Mn	Ni	Pb	Sn	Ti
% NFA57-702	≤0,35	6,5÷7,5	≤0,1	≤0,1	0,25÷0,4	≤0,3	≤0,05	≤0,05	≤0,05	0,1÷0,2

From this composition obtains:

Table 3 – Chemical composition of $AlSi_9Cu_3ZnMg$ alloy

Chemical Elements	Si	Cu	Zn	Mg	Fe	Ni	Mn	Ti	Cr
% NFEN1780-1	8,92	≤2,74	≤0,69	0,42	1,07	≤0,31	≤0,26	≤0,068	≤0,067

2.2 Equipment used for the preparation of materials

The melting furnace: consists of a main cover and a metal shell surrounded by two layers, the first in insulating concrete and the second in refractory concrete, each 150 mm thick. Inside the ferrule, three refractory bricks forming the form are placed on the furnace hearth on which rests a graphite crucible weighing 350 kg. The furnace is heated by two production gas burners and is articulated from the front (casting) to the back (charging) with its various coated accessories.

The holding furnace: With a crucible, capacity of 150 kg is built in the same way as the melting furnace with its various coated ladles made of steel.

The 50 kg graphite ladle is handled by means of a crane. The ladle is kept continuously heated all day long with a gas burner beforehand and is filled directly from the melting furnace in the front position. From this ladle, which is mounted on a swivel support and usually equipped with a hand wheel, the moulds prepared for this purpose are poured or the holding furnace is filled.

The melting and holding furnaces as well as the ladle must be cleaned and burnt periodically using appropriate equipment.

The pyrometer Type K: is a standard thermocouple for measuring in a temperature range from -270 to 1372°C and has the following composition: Chromium, alloy of (NiCr) and Aluminium, alloy of (NiAl5Si) [1].

2.3 Metal melting

The melting of the metal is done in a production gas furnace, tilting from front to back, comprising a graphite crucible with a capacity of 350Kg whose charge is composed of approximately 40% (140 kg) of new ingots delivered by "Pechiney" and a mixture of 60% (210 kg) return casting jets (casting masses, vents, pouring holes and channels, rejected and defective parts ...etc.) and whose burners are properly adjusted.

Once the total melt has become liquid at about 700°C, the first deslaggingis carried out and a first spectrometry specimen is taken for immediate chemical analysis. From the results of this analysis, the first correction is made. To correct the loss on ignition of Magnesium due to melting, a percentage of $AlMg_{10}$ is added, to readjust the Silicon, Copper and Zinc content due to the impoverishment of the casting jets, a quantity (percentage) is introduced respectively using main alloys in the form of new ingots of $AlSi_{22}$, $AlCu_{10}$ and $AlZn_{10}$ delivered by "Pechiney" to obtain an exact configuration of $AlSi_9Cu_3ZnMg$.

The liquid mass then undergoes a degassing treatment by introducing two tablets of 200g each of coveral 701 SM at a temperature of about 710°C, followed by deslagging and covering with a powder called coveral 55 in the oven. Then the metal is poured into a preheating ladle where a third deslagging and refining operation is carried out. The purpose of this refining operation is to modify the texture and orientation of the silicon crystals in order to refine the structure. This is done in the ladle at a temperature of between 730 and 750°C and is essential to obtain good mechanical characteristics. A second specimen is made to check the correction effect. If the results of the analysis of this second test specimen are correct, the bags filled with refined liquid must be sent to fill the 150 Kg holding furnace, which is poured into the prepared shell using a ladle. In order to avoid inclusions, impurities and any quantity of alumina layer remaining after several skimmings', filters, generally made of glass cloth, are carefully inserted into the moulds at the pouring channels. The casting temperature varies

according to the thickness of the part and is generally between 680 and 750 °C. The casting process is carried out by gravity. Once the specimens have been poured into moulds by gravity, the solidified metal is said to be as-cast and noted: F.

2.4 Remolding process

After the $AlSi_9Cu_3ZnMg$ alloy has solidified in the mould, the specimens are taken directly to the finishing station to separate the casting system from the spruces, and to the grinding and finishing station where the surfaces of the parts are ground and their dimensions are checked [1].

2.5 Shell casting

In this method of moulding, the mould, consists of two steel screeds (5% chromium), whose role is to maintain the impressions. These clevises, separated by a parting line, may need to be prepared and heated to a temperature of 200 to 300°C using a gas burner to allow the molten liquid mass to completely occupy the volume of the cavity in order to avoid any volume defects in terms of cracking and shrinkage. In order to increase the fluidity and flowability of the liquid metal inside the cavities, they can be surface treated.

2.6 Different phases of the heat treatment

Before starting any treatment, five tensile, impact and two as-cast samples should be taken as a reference. The remaining samples and specimens will undergo the following four heat treatments:

a) Solution heating at a homogenisation temperature closer to the eutectic temperature of the alloy, as it allows rapid diffusion of the solute elements (Si, Cu, Zn, Mg) in the Aluminium matrix.

The specimens are heated to 500°C and then held at this same constant temperature for ten hours.

As the alloy is still in the solid state, diffusion phenomena in the solid state are not instantaneous and the part must be kept at this temperature for a significant period of time (10 hours), which must be long enough for the silicon present in the intergrain spaces (richer in Si) in the as-cast state to be able to diffuse equitably towards the interior of the material. This is because during heating, the surface of the workpiece heats up more quickly than the core of the metal. In our case, a forced ventilation furnace was used to homogenise the temperature, which is checked regularly with a pyrometer.

b) Quenching treatment: at the end of the homogenisation cycle, the specimens and samples are immersed in a tank filled with water at room temperature. After quenching, the microstructure of the studied material is homogeneous and becomes finer with a notable increase in grain boundaries and precipitation of Al_2Cu, $MgZn_2$, etc. inside the grains, which are strong obstacles to dislocation sliding. This quenching generates a residual stress field within the alloy. For a more homogeneous distribution of this field and in order to obtain a uniform structure, the material was subjected to different ripenings in ambient air (20 to 25°C) followed immediately by respective temperings.

This operation consists of ensuring by appropriate cooling that the solid solution is kept in a supersaturated state. Quenching must be sufficiently fast ($\leq$ 12 seconds), to avoid a coarse precipitation of the defined compound (critical quenching speed). The test specimens are never used immediately after quenching because of their fragility, hence the need to perform a ripening treatment immediately followed by an appropriate tempering.

c) Ripening at room temperature for a period of time. Once the specimens and samples have been quenched, they are left out in the open air to undergo a natural ageing process called ripening. In our case we have varied the ripening time in 2 hours increments after quenching with the different ripenings: 0, 2, 4, 6, 8, 10, 12, 14, 16, 18, 20, 22 and 24 hours, immediately followed by the same quenching for each of the 13 respective cases.

d) Tempering: This treatment is carried out on specimens that have undergone quenching followed by ripening to reduce the brittleness due to the quenching by softening and eliminating internal stresses. Tempering is carried out for 6 hours at a temperature of 165°C.

The heat treatments applied to the alloy cause on the one hand a hardening by refining the grain size. The smaller the grain size, the larger the grain joint area per unit volume of material, the more obstacles there are to the dislocation movement. On the other hand the formations of precipitates (Mg_2Si, Al_2Cu, Al_2CuMg, $MgZn_2$ etc.) outside the solid solution: coherent, semi-coherent or incoherent with the aluminium matrix. The effect caused is the same on the deformation difficulty of the network. These precipitates are arranged along the grain joints, in the master matrix of the alloy and act as a barrier to the

movement of the dislocations, thus increasing the resistance of the alloy.

Once the heat treatments have been carried out, the material will be subjected to various tests at low loads and speeds and observations at room temperature [17-22].

3 Results and comparative study

We mainly used different techniques:

- Tension to identify the different stresses and ductility. During loading, there are initial dislocations (generally, the generation of dislocations in the same alloy under the effect of stresses are of the same sign which push). It will be necessary to develop an additional constraint to make the dislocations move in the vicinity of the others to enable them to overcome the various obstacles encountered and to move from one obstacle to another.

- The different free energies of deformation, which give information on the mode of rupture,
- The stress intensity factor KI which quantitatively characterises the resistance of a material to the abrupt propagation of a mode I crack,
- The Brinell hardness HB and microhardness $Hv_{0.05}$ to determine the stress field strength,
- Kcv resilience to assess impact resistance,
- And the microstructure to recognise the different structures.

In the following we will describe and present in detail the main mechanical characteristics obtained from the studied material $AlSi_9Cu_3ZnMg$.

The average values of the mechanical strength characteristics of the $AlSi_9Cu_3ZnMg$ alloy are shown in the following figures. They are obtained by means of a series of measurements on five identical specimens.

The cast $AlSi_9Cu_3ZnMg$ alloy is gravitationally die cast in different states with: a - as-cast noted: F, b - quenched noted: T and matured noted: c - M0h, d - M2h, e - M4h, f - M6h, g - M8h, h - M10h, i - M12h, j - M14h, k - M16h, l - M18h, m - M20h, n - M22h, o - M24h and (p) - comparison of the 15 corresponding states.

It is reported that the matured state M0h has in fact undergone a tempering while the quenched state T has remained in its initial quenched state.

3.1 Influence of $AlSi_9Cu_3ZnMg$ alloy state on the tensile strength

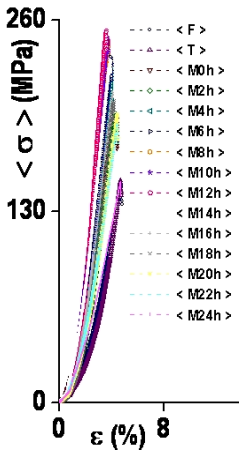

Fig.1 – Stress – strain curves of the $AlSi_9Cu_3ZnMg$ alloy with σ: average stress, ε (%): strain.

Figure.1 shows a comparison of the average curves (stress-strain) of the fifteen states of the $AlSi_9Cu_3ZnMg$ alloy in order to determine a suitable compromise.

The elastic, plastic and stress characteristics, the stress intensity factor Ks and the different fracture energies of the alloys are very important parameters when designing elements subject to external stresses in general and mechanical stresses in particular. In fact, the elastic limit sets the permissible value that must not be exceeded to prevent the manufactured parts from crossing the range of reversible to permanent deformation. Elongation and breaking load, respectively, provide information on the limit of deformability of the materials to be subjected to geometrical modifications and the estimated resistance of the material beyond which it enters the breaking phase.

All of the curves (Fig.1) obtained show almost the same shape which can be distinguished by three different regions:

a) A large linear elastic part of equation $\sigma_e = E\varepsilon_e$: This part can be explained by the movement of atoms linked by electrostatic forces. The atoms of a crystal have a natural distance for which all these forces equilibrate. The application of a weak external force disturbs this equilibrium and the atoms move away from each other until the interatomic forces cancel out the applied force. When the force is removed, the atoms return to their initial position, resulting in reversible deformation.

b) A first small homogeneous plastic section with the following shape $\sigma = K\varepsilon^n$: Before the elastic deformation reaches its limit, a second part appears, which is the plastic deformation. It is mainly carried out by a sliding of one part of the crystal with respect to the other according to an integer number of times the interreticular distance. This sliding is interpreted by the movement of the initial mobile dislocations or those created during the deformation, and their interactions with various obstacles present in the material.

c) And a second plastic part, this time heterogeneous, very restricted, showing a fragile fracture: determined by the resilience Kcv or Kcu and the stress concentration coefficient Ks. It goes through two stages; the first is the beginning of the cracks and their coalescence with the apparition of striction and the second, their propagation through the whole section of the specimen.

3.2 Influence of heat treatment on the deformation energy of the $AlSi_9Cu_3ZnMg$ alloy

Figure 2 shows the average strain free energy curves W (J) - C (mm) for $AlSi_9Cu_3ZnMg$ alloy. This is a comparison of the curves (Energy - Stroke) of the fifteen states of the $AlSi_9Cu_3ZnMg$ casting alloy to determine the free strain energy trade-off.

The study of the curves (Fig.2) previously mentioned has made it possible to determine the different energies of each state of the $AlSi_9Cu_3ZnMg$ casting alloy.

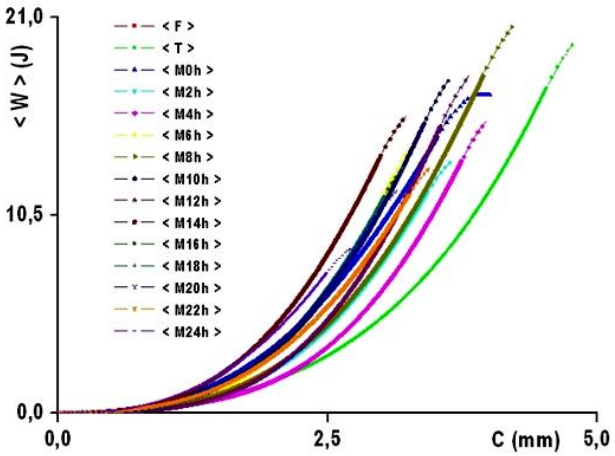

Fig. 2 – Mean curves of: free strain energy W(J) - Mean Stroke C(mm)

3.3 Influence of the ripening time on resistance and hardness characteristics

The following figures show the variation of the various resistance and hardness characteristics as function of the ripening time t. Non-measurable coefficients are determined by inverse identification procedures.

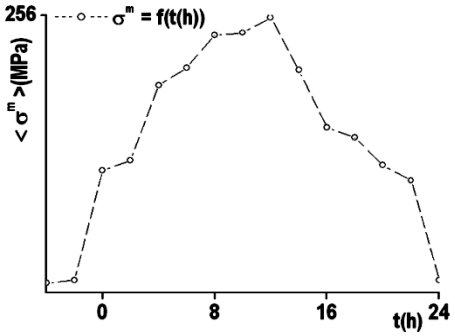

Fig. 3 – Maximum stress σ^m – ripening time t

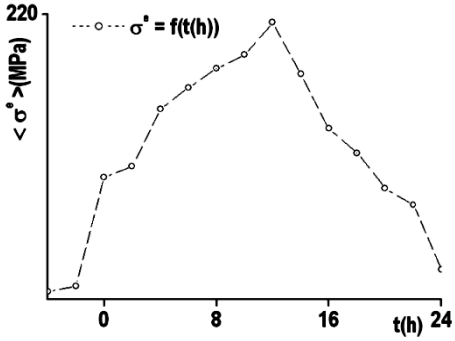

Fig. 4 – Elasticity stress σ^e – ripening time t

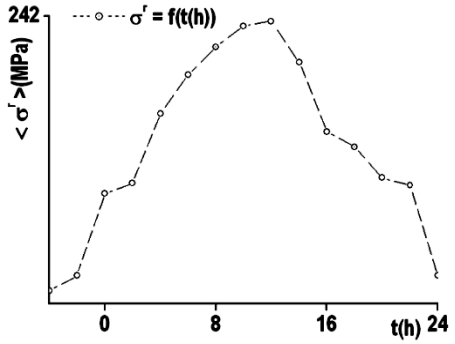

Fig. 5 – Breaking stress σ^r – ripening time t.

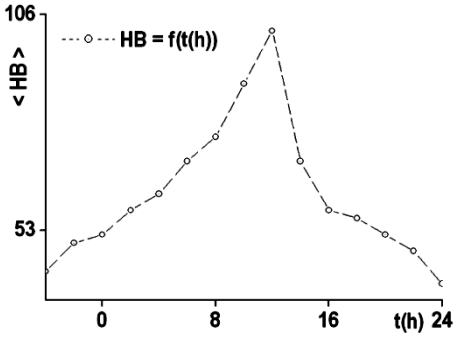

Fig. 6 – Brinell hardness HB – ripening time t.

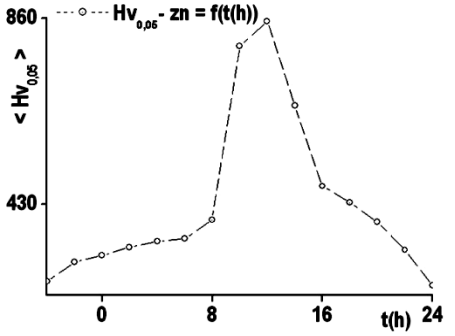

Fig. 7 – Microhardness of the black zone $Hv_{0,05}$-Zn – ripening time t.

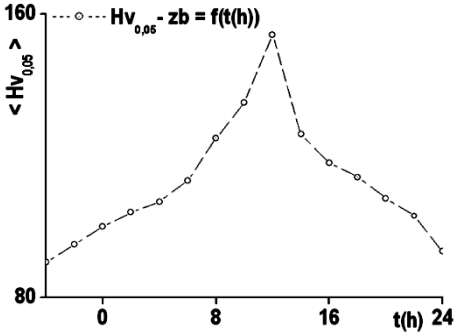

Fig. 8 – Microhardness of the white zone $Hv_{0,05}$-Zb – ripening time t.

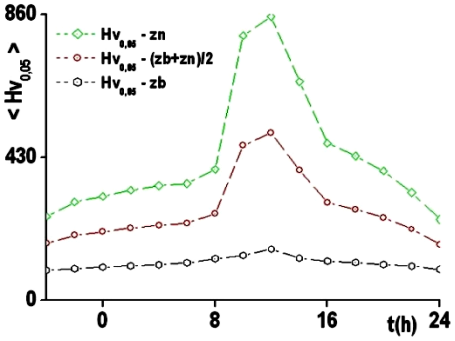

Fig. 9 – comparison of the Vickers microhardness of the black zones noted: Zn, white zones noted: Zb and their mean noted (Zb+Zn)/2 - ripening time t

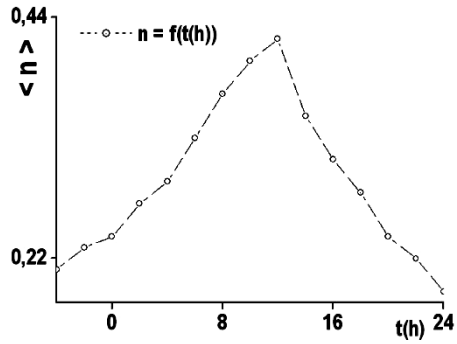

Fig. 10 – Strain-hardening coefficient n - ripening time t.

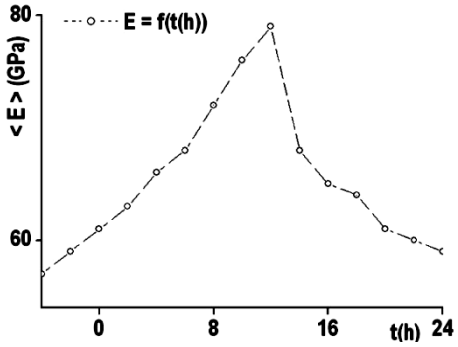

Fig. 11 – Young's modulus E - ripening time t.

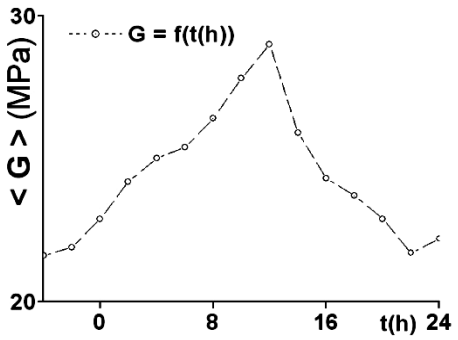

Fig. 12 – Shear modulus G - ripening time t.

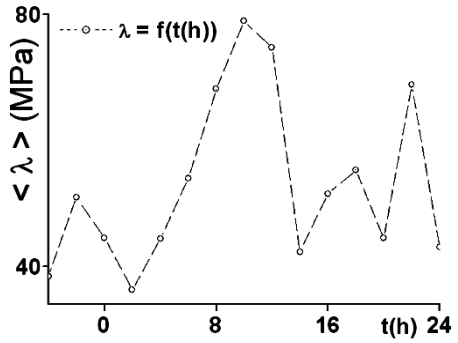

Fig. 13 – Lamé Coefficient λ – ripening time t.

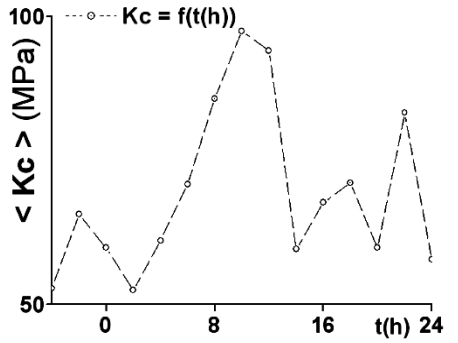

Fig. 14 – Hydrostatic compressive modulus Kc – ripening time t.

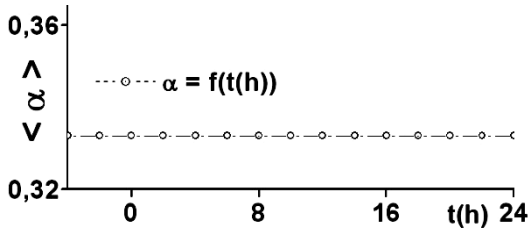

Fig. 15 – Coefficient of thermal linear expansion α – ripening time t.

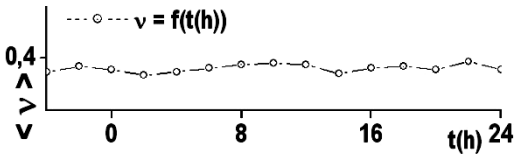

Fig. 16 – Poisson Coefficient ν – ripening time t.

3.4 Influence of ripening time on ductility

The following figures show the variation of the ductility parameters as function of the ripening time t

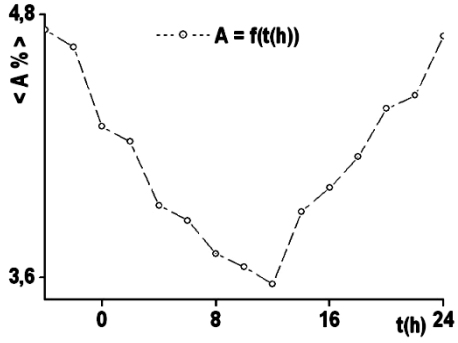

Fig. 17 – Percentage elongation A% – ripening time t.

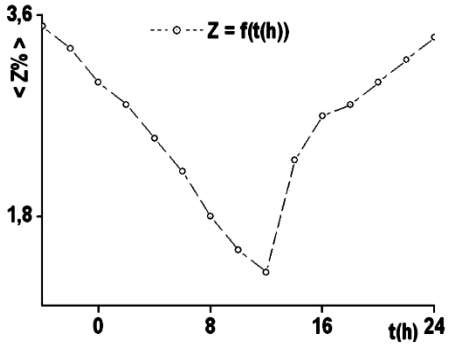

Fig. 18 – Striction Coefficient Z% – ripening time t.

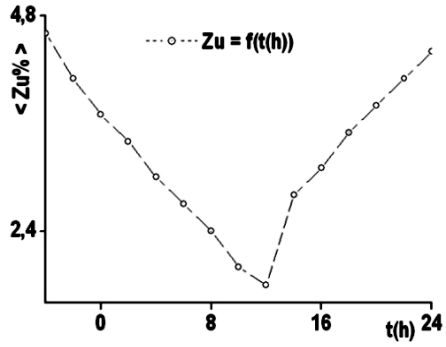

Fig. 19 – Stress elongation Zu% – ripening time t.

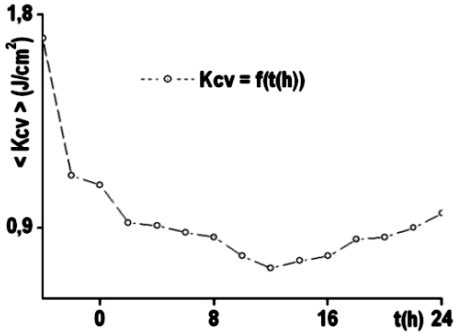

Fig. 20 – Resilience Kcv – ripening time t.

3.5 Influence of ripening time on the free energies of deformation

The following figures show the variation of the various energies and the stress intensity factor as function of the ripening time t

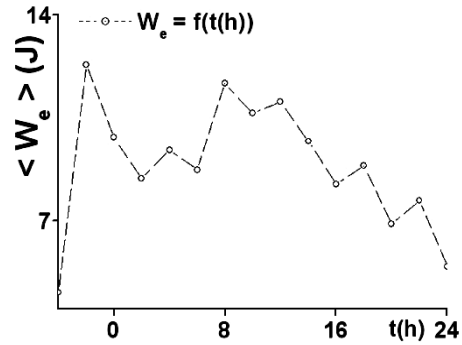

Fig. 21– Energy of elastic deformation We – ripening time t.

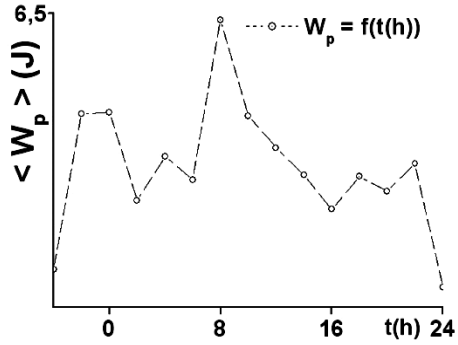

Fig. 22 – Plastic deformation energy Wp – ripening time t.

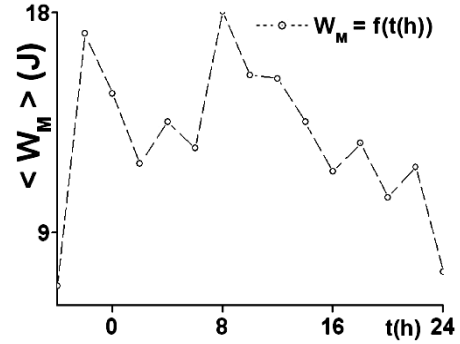

Fig. 23 – Maximum strain energy W_M – ripening time t.

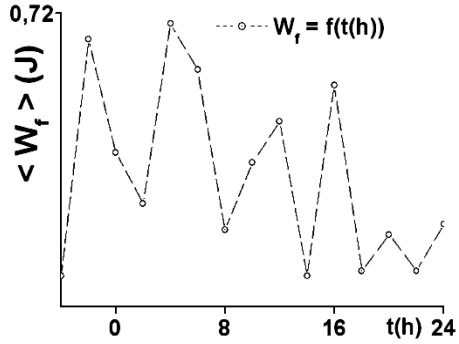

Fig. 24 – Crack deformation energy Wf – ripening time t.

4 Discussion

In this type of gravity die-casting, the average curve of the M12h state is above all the curves of the other states (Fig. 1) The mechanical properties of extrinsic strength which are σ^m, σ^e, σ^r, HB, $Hv_{0.05}$, n, E, G, λ and Kc increase abruptly from the as-cast F (minimum strength properties) to the quenched state with an incoherent distribution of precipitates. This evolution passes through the M6h state with semi-coherent precipitates to reach the maximum value in the M12h state with coherent precipitates and a maximum compromise of strength and ductility properties to then decrease to M18h (semi-coherent

precipitates) to finally reach the final state M24h (incoherent precipitates and minimum strength properties) Figs. 3 to 14. This is to the detriment of the extrinsic mechanical ductility properties A%, Z%, Zu%, Kcv, and the various free energies of deformation, which decrease abruptly respectively from the as-cast state F (maximum ductility properties) to the M12h state (minimum ductility properties) and finally increase to M24h (maximum ductility properties) Figs. 17 to 25. However, the rate of growth or decay differs from one property to another. On the other hand, the intrinsic characteristics which are the coefficient of linear thermal expansion α and the fish coefficient ν remain almost invariant Figs. 15 and 16.

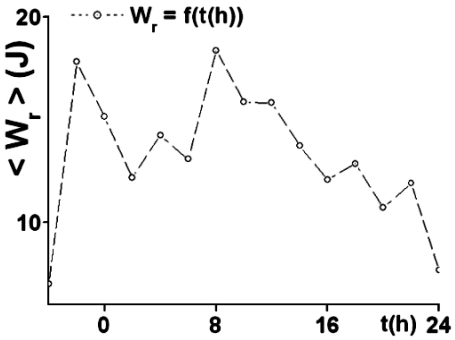

Fig. 25 – Total deformation energy or breaking energy W r – ripening time t.

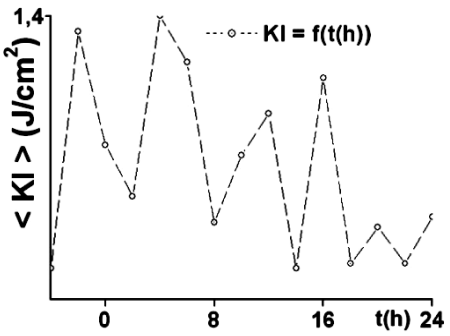

Fig. 26 – Stress intensity factor KI – ripening time t.

It can be seen that the strengths (Figs. 3 to 14) of the alloy in the ripening state M12h are higher than those of the other states at the detriment of ductility (Figs. 17 to 25). Analysis of these results shows that the compromise is the M12h state for parts of any strength state, as the natural ageing process was completed after 12 hours of ripening followed by complete tempering at 165°C for 6 hours.

In figures 7 to 9, the graph of the microhardness of the black zone is clearly above that of the microhardness of the white zone in all states.

The black zone is probably the solid solution of aluminium, copper, zinc and magnesium in silicon, while the white zone is the solid solution of silicon, copper, zinc and magnesium in aluminium.

5 Microstructure study of the $AlSi_9Cu_3ZnMg$ die-cast alloy as a function of the state of maturation

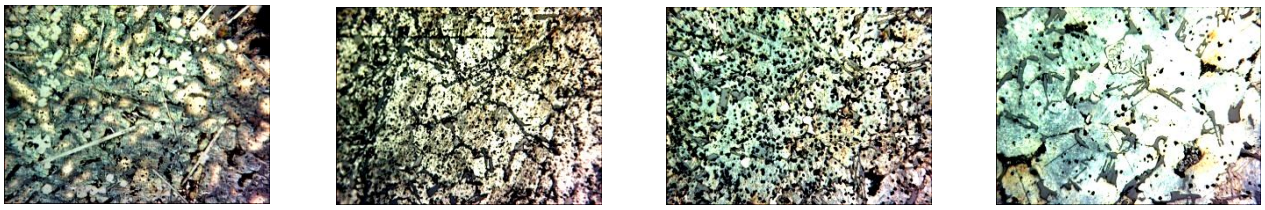

(a) Fx200 (b) M0hx200 (c) M12hx200 (d) M24hx200

Fig. 27 – Micrographic structures of the casting alloy $AlSi_9Cu_3ZnMg$accordingto the state of ripeness

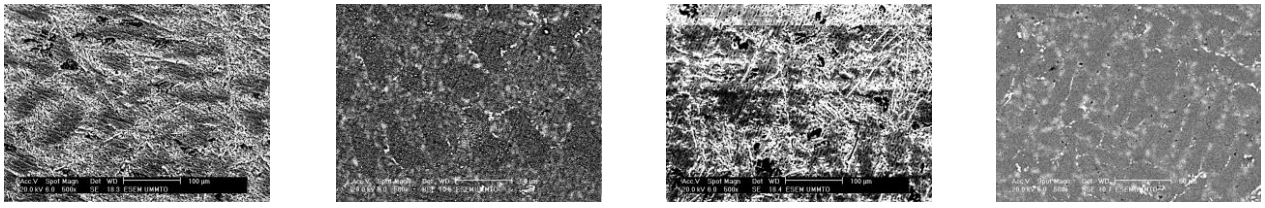

(a) F (b) M0h (c) M12h (d) M24h

Fig. 28 – SEM microstructures of the casting alloy $AlSi_9Cu_3ZnMg$ according to the state of maturat ion

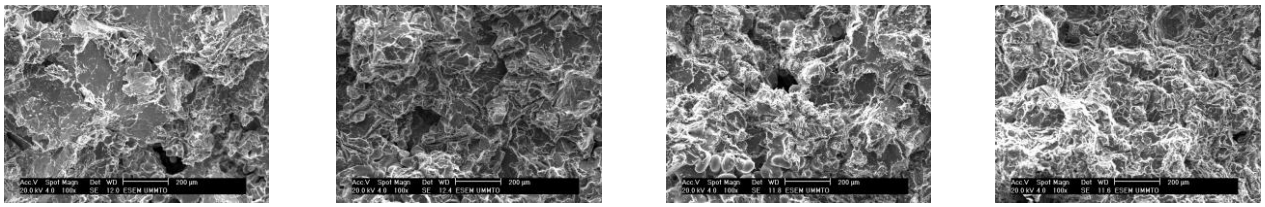

(a) F (b) M0h (c) M12h (d) M24h

Fig. 29 – SEM tensile fracture toughness of $AlSi_9Cu_3ZnMg$ according to the state of maturation

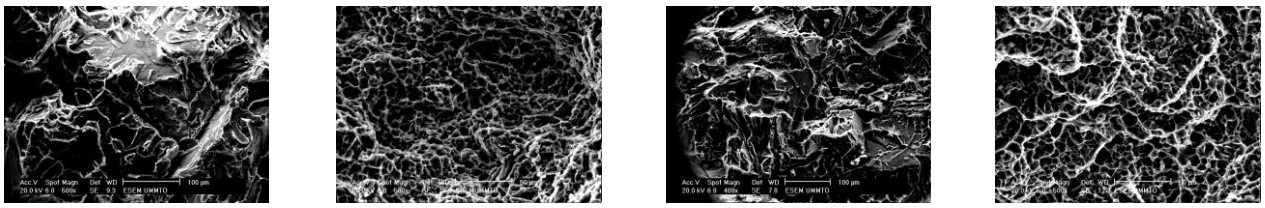

(a) F (b) M0h (c) M12h (d) M24h

Fig. 30 – SEM impact fracture toughness of $AlSi_9Cu_3ZnMg$ according to the state of maturation

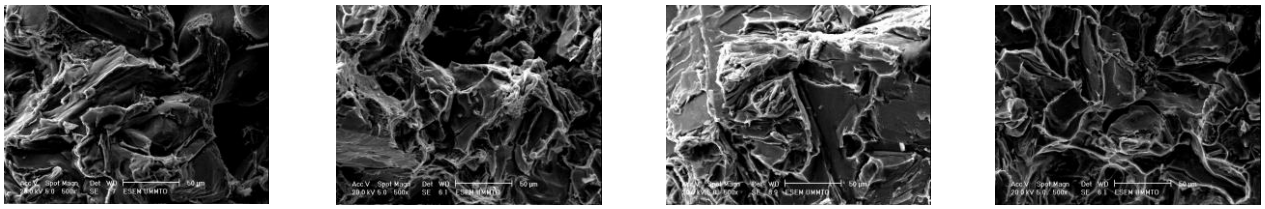

(a) F (b) M0h (c) M12h (d) M24h

Fig. 31 – SEM flexural fracture toughness of the $AlSi_9Cu_3ZnMg$ as a function of the state of maturation

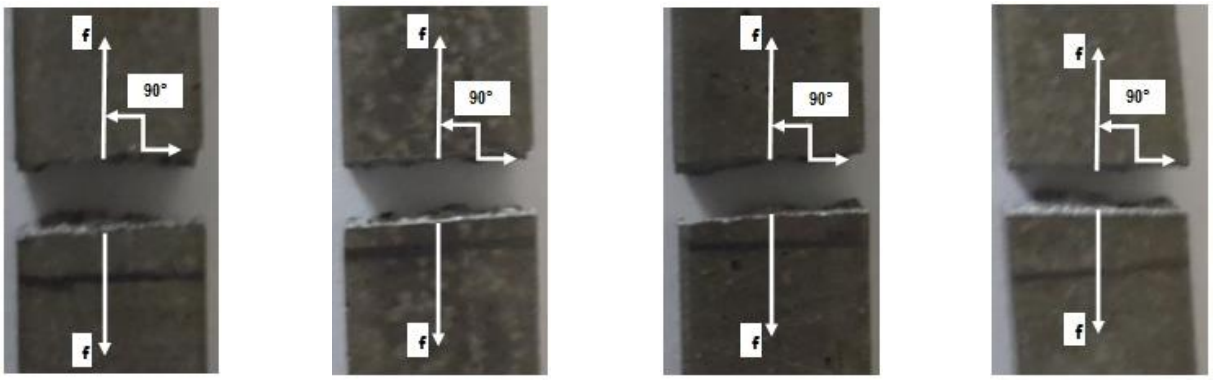

(a) F (b) M0h (c) M12h (d) M24h

Fig. 32 – Brittle fractures at 90° to the tensile axis of $AlSi_9Cu_3ZnMg$ depending on the state of maturation with f - traction force.

The different figures show that:

– The fracture deformations as well as the different free deformation energies Figs. 21 to 25 are very low because the damage occurred in a sudden manner.

– The elongations at break A% is less than 5% (Fig. 17),

– The values of the Z - striction coefficients are below 0,1 (Fig.18),

– Kcv resilience is very low (Fig.20),

– The fracture (Fig. 29), tensile (Fig. 30) and flexural (Fig. 31) fracture faces have a grainy, shiny appearance,

– The stress intensity factor KI (Fig. 26) which quantitatively characterises the resistance of the alloy to the sudden propagation of a crack in mode I is very low,

– The fracture energy of the crack is very low (Fig.24), when the specimen is loaded, it has a horizontal fracture surface (Fig.32), as the shear stress is maximum in horizontal planes of 90° to the line of the applied tensile force.

These eight criteria and observations show us that the fracture is substantially represented by a topographic facies characteristic of an intergranular brittle fracture highly dependent on the morphological structure of the $AlSi_9Cu_3ZnMg$ alloy grains. In this case, the fracture mode is probably type I (with very low KI (Fig. 26)) with severe loading perpendicular to the plane of the crack.

In metal moulds, solidification occurs much faster, resulting in a finer structure Fig.27 (a) (F). The grain size of the metal has a significant effect on its mechanical properties. These properties, especially its ductility and plasticity, are more pronounced when the structure is finer, because the smaller the grain size, the more obstacles there are to the movement of dislocations.

In the as-cast state, the studied alloy $AlSi_9Cu_3ZnMg$ generally contains large, randomly distributed grains which are produced after solidification and in which the distribution of the contents of the different addition elements (Si, Cu, Zn and Mg) is non-uniform. This leads to the creation of structural and local heterogeneities which generate a stress field that varies from one point to another in the material, in the latter, there are regions that are difficult to deform and others that are easily deformable. Consequently, during external mechanical stress, the deformation appears first of all in the regions that are favourable to the sliding of dislocations. In order to improve the mechanical characteristics of the alloy under study, it is necessary to hinder the movement of dislocations throughout the material by causing the formation of a fine structure and finely dispersed precipitates (Mg_2Si, Al_2Cu, Al_2CuMg, $MgZn_2$, Al, Si, Cu, Zn, Mg etc.), for this reason we have carried out a specific heat treatment on the alloy which is performed in four stages. The microstructure of the studied alloy in the as-cast states shows a rather heterogeneous distribution of the different additive elements (Si, Cu, Zn and Mg), but their repartition in the matrix in the matured and tempered states is homogeneous. When analysing the microstructures Figs. (27, 28)((a), (b), (c), (d)), we noticed that the grain size decreases from the as-cast state F (heterogeneous coarse grains) through the M0h state (homogeneous coarse grains) to the M12h state (homogeneous fine grains) to the M24h state with a homogeneous structure and very large grains, which explains the evolution of strength and ductility Fig. 3 to 26.

6 Sequences of the precipitation

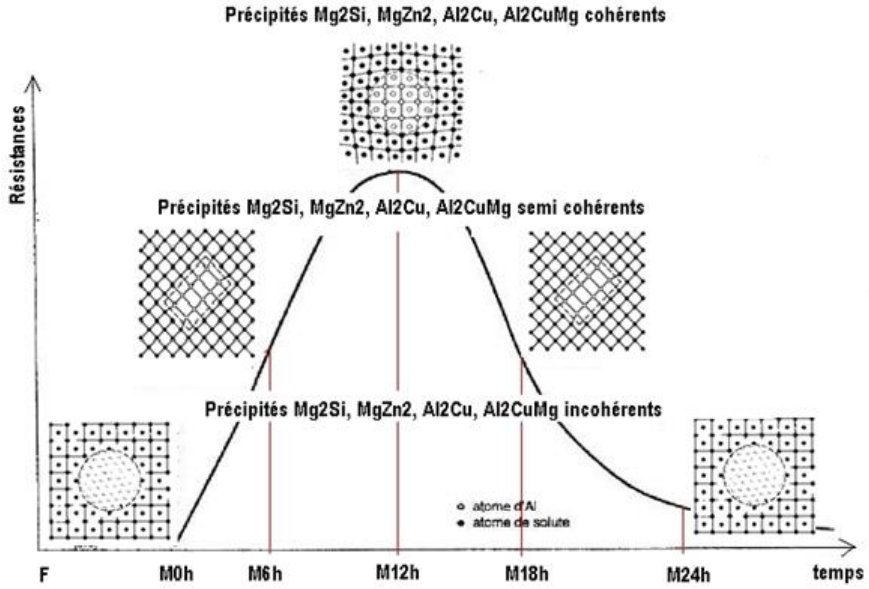

Fig. 33 – Sequences of the precipitation of the $AlSi_9Cu_3ZnMg$ alloy

The $AlSi_9Cu_3ZnMg$ alloy presents four kinds of precipitates of type Mg_2Si, Al_2Cu, Al_2CuMg, $MgZn_2$ etc.

7 Conclusion

Observation under a scanning electron microscope reveals in the alloy studied, on the one hand, in quenched state, inter-granular and transgranular precipitates of the Al_2Cu type, on the other hand in matured states, homogeneous intra-granular precipitates of the kind (Mg_2Si, $MgZn_2$ and Al_2CuMg). All the corresponding curves reported on the same graph show us that the curve of the state < M12h > is far above all those of the other states.

the graphs of the stresses, the Brinell hardness, the microhardness, the Young's modulus, the coefficient of consolidation and the different strain energies as a function of the maturation time increase from the as-cast state to the state < M0h > (incoherent precipitates with minimal resistance properties) then < M6h > with (semi-coherent precipitates presenting average resistance properties) to finally grow from the latter and reach the maximum value at the state < M12h > (coherent precipitates with properties of maximum resistances) to then decrease to < M18h > (semi coherent precipitates with average resistance properties) then < M24h > with (incoherent precipitates with minimal resistance properties) **(**Fig.33) to the detriment of elongations, necking and resilience. While the intrinsic Poisson's ratio remains practically invariant. The speed of growth or decline is different from one property to another. It turns out that the extrinsic values of the breaking strength, the tensile strength, the yield strength, the Brinell hardness, the Vickers microhardness, the Young's modulus, the consolidation coefficient and the different strain energies of the alloy in the matured state < M12h > are higher than those of the other states. The analysis of these results shows us that the compromise is the state < M12h > for resistance parts whatever the states considered because the aging process is completed after a well-chosen maturation time followed by a complete tempering at a well-determined temperature and duration.

In order to meet manufacturers' requirements for a rational use of this alloy, it is preferable to develop the various parts for use under different stresses in gravitationally cast metal moulds followed by a 12 hours ripening for the strength parts. As a result, $AlSi_9Cu_3ZnMg$ is a heat-treated casting alloy with good cast ability.

REFERENCES

[1]- A. Hakem. Effet du mode d'élaboration et de maturation sur les proprietes mecaniques et la microstructure des alliages de fonderie Al Si. Thèse de doctorat. Universite Mouloud MAMMERI Tizi-Ouzou, Algerie 2014.

[2]- M. Colombié, D. Albert, Matériaux industriels: Matériaux métalliques. Dunod, 2000.

[3]- J.-P. Baillon, J.-M. Dorlo, Des Matériaux. Ecole Polytechnique de Montréal, Montréal, 2000.

[4]- D. François, Essais mécaniques et lois de comportement. Hermès, (2001).

[5]- A. Cornet, F. Hlawka, Propriétés et comportements des matériaux: du microscopique au macroscopique. Ellipses, 2010.

[6]- D.R. Askeland, The science and engineering of materials. Third Edition ed.: PWS Publishing Company Boston, 2003.

[7]- M.F. Ashby, D.R. Jones, Y. Brechet, J. Courbon, M. Dupeux, Matériaux: Microstructure et mise en øeuvre. Dunod, 1991.

[8]- F. Condet, A. Reynaud, Atlas der Metallographie von Gusseisen. Editions Techniques des Industries de la Fonderie, (2009).

[9]- M. Garat, A. Le Nézat, M3637 - Moulage des alliages d'aluminium-Moules permanents: coquille, sous pression et apparentés. Techniques de l'Ingénieur, traité Matériaux métalliques, (2013). doi:10.51257/a-v2-m3637.

[10]- M. Garat, M3635 - Fusion des alliages d'aluminium. Techniques de l'Ingénieur, traité Matériaux métalliques, (2012). doi:10.51257/a-v2-m3637.

[11]- R. Portalier, M810A - Fonderie et moulage des alliages d'aluminium. Techniques de l'Ingénieur, traité Matériaux métalliques, (1990). doi:10.51257/a-v2-m3637.

[12]- M. Garat, M4675 - Propriétés des alliages d'aluminium de fonderie. Techniques de l'Ingénieur, traité Matériaux métalliques, (2012). doi:10.51257/a-v2-m3637.

[13]- J.-B. Leblond, P. Germain, Mécanique de la rupture fragile et ductile. Hermès science publications, 2003.

[14]- A. Pokorny, J. Pokorny, M4122 - Fractographie. Macrographies et micrographies. Techniques de l'ingénieur. Matériaux métalliques, (2003) 1-M4122. 14.

[15]- A. Hakem, Influence of ripening on the evolution of mechanical and structural properties of the AlSi12Cu1Mg alloy. J. Mat. Eng. Str. «JMES», 4(4) (2017) 245-257.

[16]- A. Hakem, Influence of the tempering on the evolution of the mechanical characteristics and microstructure of the

foundry alloy AlSi7Zn3Cu2Mg. J. Mat. Eng. Str. «JMES», 5(3) (2018) 289-304.
[17]- C. Meyers, Solution heat treatment effects in A357 alloys. AFS Trans, 93 (1985) 741-750.
[18]- Y. Desalos, M1105 - Introduction aux traitements thermiques des métaux et alliages. Techniques de l'Ingénieur, traité Matériaux métalliques, (2003). doi:10.51257/a-v2-m3637.
[19]- Y. Desalos, M1110 - Panorama métallurgique des traitements thermiques. Techniques de l'Ingénieur, traité Matériaux métalliques, (2003). doi:10.51257/a-v2-m3637.
[20]- R. Develay, M1290 - Traitements thermiques des alliages d'aluminium, Techniques de l'Ingénieur, traité Matériaux métalliques. (1986).
[21]- G. Lesoult, M58 - Solidification - Cristallisation et microstructures Techniques de l'Ingénieur. Traité Matériaux métalliques. (1986). doi:10.51257/a-v1-m58.
[22]- A. Hakem, A. Hakem, Y. Bouafia, Study of Behavior and the Damage in Tensile and with the Shock of the Eutectic Alloy AlSi13Mg Unstandardized. Mater. Today: Proc., 2(10, Part A) (2015) 4984-4991. doi:10.1016/j.matpr.2015.10.087.
[23]- D. Bruno, S. Pierre, M240 - Durcissement par précipitation des alliages d'aluminium Techniques de l'Ingénieur. Traité Matériaux métalliques. (1991). doi:10.51257/a-v1-m240.
[24]- J. Lendvai, Precipitation Processes in Age-Hardenable Aluminium Alloys, in Advanced Light Alloys and Composites, R. Ciach, Editor. Springer Netherlands: Dordrecht. (1998), 307-318. doi:10.1007/978-94-015-9068-6_39.
[25]- J.-L. Martin, Dislocations et plasticité des cristaux. Vol. 5. Lausanne: Presses Polytechniques et Universitaires Romandes, 2000.
[26]- Z. Zhuang, Z. Liu, Y. Cui, Dislocation Mechanism-Based Crystal Plasticity, Z. Zhuang, Z. Liu,Y. Cui, Editors, Academic Press. (2019). doi:https://doi.org/10.1016/B978-0-12-814591-3.00001-7.
[27]- J.G. Kaufman, E.L. Rooy, Aluminum alloy castings: properties, processes, and applications. Asm International, 2004.
[28]- C. Vargel, M4661 - Propriétés générales de l'aluminium et de ses alliages. Techniques de l'ingénieur. Matériaux métalliques, (2005).
[29]- J. Barralis, G. Maeder, Précis de métallurgie: élaboration, structures-propriétés et normalisation. 6e édition ed. Paris: Nathan : AFNOR, 1991.